Hindawi
Geofluids
Volume 2022, Article ID 6006383, 17 pages
https://doi.org/10.1155/2022/6006383

Research Article

Numerical Research of Lightweight Foam Concrete Replacement Method of Deep Soft Foundation Treatment of Low-Filled Embankment

Fanfan Li,[1] **Zhifeng Zhang**,[1] **Xing Chen**,[1] **Zecheng Chi**,[2] **Jianbin Li**,[3] **and Wei Wang**[4]

[1]*Research and Development Center on Technology and Equipment for Energy Conservation and Environmental Protection of Highway Transport, Anhui Transport Consulting & Design Institute Co., Ltd, Hefei 230088, China*
[2]*Faculty of Engineering, China University of Geosciences, Wuhan 430074, China*
[3]*School of Civil Engineering, Guangzhou University, Guangzhou 510006, China*
[4]*Guangdong Research Institute of Water Resources and Hydropower, Guangzhou 510610, China*

Correspondence should be addressed to Zecheng Chi; chizecheng@cug.edu.cn

Received 7 March 2022; Accepted 19 May 2022; Published 13 June 2022

Academic Editor: Zizheng Guo

A new method of replacing soft soil with lightweight foam concrete (lightweight foam concrete replacement method, LFCRM) is carried out to treat deep soft foundation under the low-filled embankment. Two-dimensional models with different thicknesses of replacement are established by the finite element platform (MIDAS/GTS). Moreover, the deformation and stress distribution law of treated foundation is analyzed by numerical simulation with different models. The results are as follows: (1) LFCRM can offset part of dead load; (2) the transverse distribution of settlement presents an "arc" shape; (3) the replacement made of lightweight foam concrete can spread stress well; (4) increase of replacement thickness will cause the necking of the additional stress "bubble"; (5) initial excess pore water pressure is related to the additional stress, and its dissipation path is deduced; (6) preliminary analysis indicates the feasibility of LFCRM for treating deep soft foundation with the low-filled embankment.

1. Introduction

Soft foundation failure is one of the most common geotechnical problems [1–3]. Deep soft soil is widely distributed in the plains of China [4], and low-filled embankment is a common form of road construction in this region because of the conservation of land resources [5]. Conventionally, a deep soft foundation in road engineering can be treated by the composite foundation, rigid pile, and drainage consolidation method [6–8]. Related specifications suggest that the treating depth of the above methods should be greater than that of soft soil [9], which is, however, not economical for the low-filled embankment.

Improvements have been made on existing methods to improve economic benefits in treating deep soft foundation under the low-filled embankment, such as composite foundation by partial penetration of columns [10–12], silt extrusion by riprap dumping [13], and shallow drainage consolidation method [14–16].

Methods for deep soft foundation treatment with low-filled embankment are far more than above [17–19]. Interestingly, these methods share similar basic mechanisms: (1) changing the physical properties (increasing elasticity modulus) of the top layer of soft soil (area with the largest additional stress) by physical, chemical, or biological method [20, 21] to reduce the

deformation of top layer and (2) turning the foundation to the double-layered structure (the upper layer is harder than the lower layer) and accordingly changing the distribution of additional stress (a harder layer can effectively spread the upper load [22]).

In this paper, treating deep soft foundation with low-filled embankment is considered by replacing soft soil with lightweight foam concrete (lightweight foam concrete replacement method, LFCRM). Except for the above advantages, this method can also offset part of dead load by the density difference between the two materials.

Tam et al. [23] studied the physical property of foam concrete with different densities (1300-2250 kg/m^3) and concluded that the strength of moist-cured foam concrete depends on both water/cement ratio and air/cement ratio. Nambiar and Ramamurthy [24] measured the water absorption of foam concrete by complete immersion for various mixes with different fly ash replacement levels for sand and different foam volume. It was found that sorption values are lower than the corresponding base mix (without foam) and reduce with the increase in foam volume. Bing et al. [25] represented that foam concretes with a density of 800-1500 kg/m^3 and compressive strength of 10-50 MPa (28 days) can be made using silica fume, fly ash, and polypropylene fiber. Ranjani and Ramamurthy [26] examined the behavior of foam concrete produced with two synthetic surfactants under sodium and magnesium sulfate environment. They indicated that the expansion of foam concrete exposed to sodium sulfate is 28% higher than that exposed to magnesium sulfate environment, which can be attributed to the greater quantum of ettringite formed in sodium sulfate environment. Wan et al. [27] studied the full field drying shrinkage distributions of foam concrete by the expanded digital volume correlation method with a high precision of 0.01 voxel (about 0.6 μm) in displacement.

Zhang and Yang [28] focused on foam concrete aircraft arresting system, which provides an economical and nondestructive means for decelerating aircraft that overshoot runway, and also conducted a full-scale test to demonstrate the effectiveness of the system. Tan et al. [29] put forward a composite support system containing foam concrete damping layer in view of the large deformation in soft rock roadway, and related application has been carried out successfully. She et al. [30] implemented continuous field testing of settlement, lateral displacement, and soil pressure in the Hangzhou East Railway Station Project and identified the excellent loading and differential settlement reduction of foam concrete as a filling material. Cai et al. [31] studied the dynamic characteristics of lightweight foam concrete with different wet densities and water-bearing states under train loading. Huang et al. [32] established a large-scale model of a subgrade filled with lightweight foam concrete with target density of 650 kg/m^3 to determine its long-term performance under cyclic dynamic loads. The results show that the strength of lightweight foam concrete with target density of 500-800 kg/m^3 can meet the requirements of both the static and dynamic conditions of ballastless track subgrade, and the ballastless track subgrade filled by lightweight foam concrete with target density of 650 kg/m^3 has a good long-term dynamic stability under cyclic dynamic loads when a dynamic buffer layer with thickness of 0.5 m is set between lightweight foam concrete layer and foundation slab. Klomranok and Su [33] conducted numerical simulations based on basic physics experiments and claimed that the presence of foam concrete in high-speed railways could reduce the dynamic response that occurs more efficiently than the traditional track structure.

There has been a great deal of research on the properties and applications of foam concrete [31, 34–36], but few of them mention LFCRM directly. This paper sheds light on the LFCRM and explores the influence of the thickness of replacement on the deformation and stress distribution of reinforced foundation (treated by LFCRM) by numerical simulation. Finally, the feasibility of LFCRM is preliminarily identified based on the results of numerical simulation and the Chinese technical specification [9, 37].

This paper is organized as follows. Section 2 introduces a newly built expressway project and describes the design and mechanism of this project. In Section 3, the numerical simulation method and two-dimensional models are constructed by finite element platform. Sections 4 and 5 analyze the deformation and stress simulation results and discuss the preliminary feasibility of LFCRM. Conclusions are summarized in Section 6.

2. Project Profile

2.1. Background. Soft soil is exposed on the ground surface in one section of a newly built expressway project, reaching a maximum depth of 21.6 m. Below it lies the strongly weathered argillaceous sandstone. The longitudinal section of geology in this section is shown in Figure 1, and the recommended geological parameters are shown in Table 1.

2.2. Design and Mechanism. In this project, the soft foundation treatment by LFCRM is considered. As shown in Figure 2, the design and mechanism are described as follows:

2.2.1. Design. The thickness of replacement is 1.5-3.0 m; the width of replacement is equal to the bottom width of the embankment; the physical parameters are shown in Table 1.

2.2.2. Mechanisms. (1) The weight difference between soft soil and lightweight foam concrete can offset part of the dead load; (2) lightweight foam concrete has a larger elasticity modulus than soft soil, reducing the deformation of the area of replacement; (3) replacing soft soil with lightweight foam concrete to form a double-layer structure (upper layer is harder than the lower) can spread the upper load effectively.

3. Numerical Simulation Method and Models

MIDAS/GTS is a software program for the stress-strain analysis and design in the construction phase of geotechnical structures [38–42]. In this study, MIDAS/GTS was used for simulation analysis, and the geotechnical parameters and material properties used in the simulation were provided from the design file of the expressway project, so that the simulation results can reflect the characteristics of the treated foundation and better guide the design.

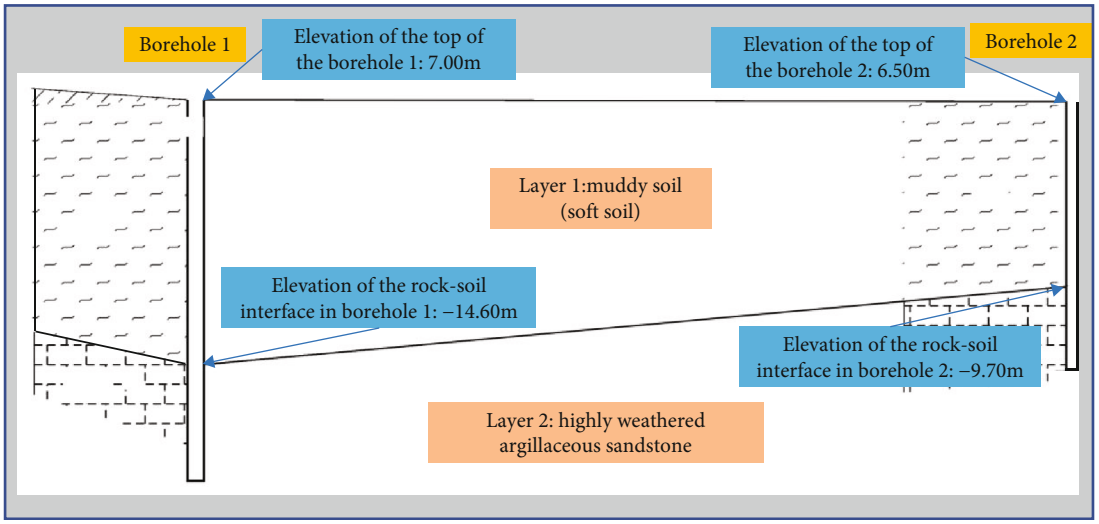

Figure 1: Longitudinal section of engineering geology.

Table 1: Parameter values of various materials.

Material	Elasticity modulus/MPa	Poisson ratio	Volume weight/ kN·m^{-3}	Permeability coefficient/m·s^{-1}	Cohesive force/kPa	Friction angle/°
Lightweight foam concrete	250	0.20	8.00	1.0×10^{-4}	120	4
Embankment	50	0.25	20.00	/	15	25
Soft soil	15	0.38	19.22	1.20×10^{-7}	12	10
Strongly weathered argillaceous sandstone	500	0.25	23.00	9.51×10^{-8}	32	30

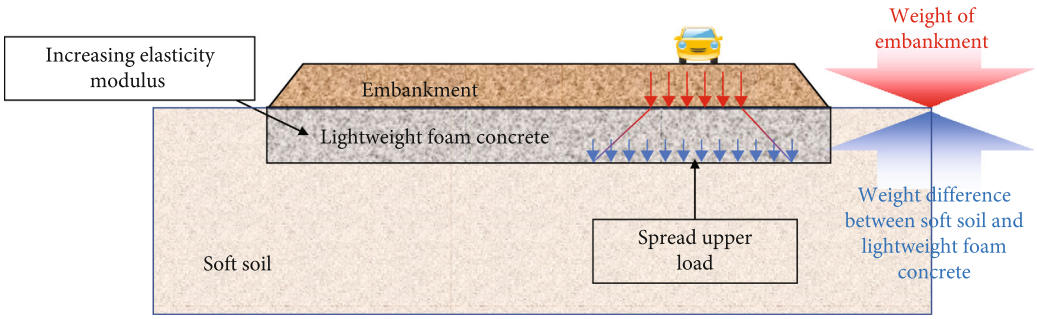

Figure 2: Scheme of the lightweight foam concrete replacement method.

3.1. Basic Theory of MIDAS/GTS

3.1.1. Finite Element Governing Equation. Based on the Hellinger-Reissner variational principle [43], the virtual work equation is obtained:

$$\delta G_{\text{ext}} = \int_{\Omega} (\nabla \delta \mathbf{u})^T \boldsymbol{\sigma} + \delta \boldsymbol{\sigma}^T (\nabla \mathbf{u} - \boldsymbol{\varepsilon}(\boldsymbol{\sigma})) d\Omega, \quad (1)$$

where G_{ext} is the virtual work generated by the external force; ∇ is the strain-displacement relational operator; $\mathbf{u}$ is the displacement; $\boldsymbol{\sigma}$ is the stress; $\boldsymbol{\varepsilon}$ is the strain; Ω is the integral area; and $\boldsymbol{\varepsilon}(\boldsymbol{\sigma})$ is the strain derived from stress.

If elements satisfy the compatibility equation of deformation, the following equation can be obtained from Equation (1):

$$\delta G_{\text{ext}} = \int_{\Omega} (\nabla \delta \mathbf{u})^T \boldsymbol{\sigma}(\mathbf{u}) d\Omega. \quad (2)$$

Equation (2) may be expressed as follows by utilizing the displacement-strain relationship:

$$\delta G_{\text{ext}} = \delta \mathbf{d}^{eT} \left[\sum \int_{\Omega} (\nabla \mathbf{N})^T \mathbf{D} (\nabla \mathbf{N}) d\Omega \right] \mathbf{d}^e, \quad (3)$$

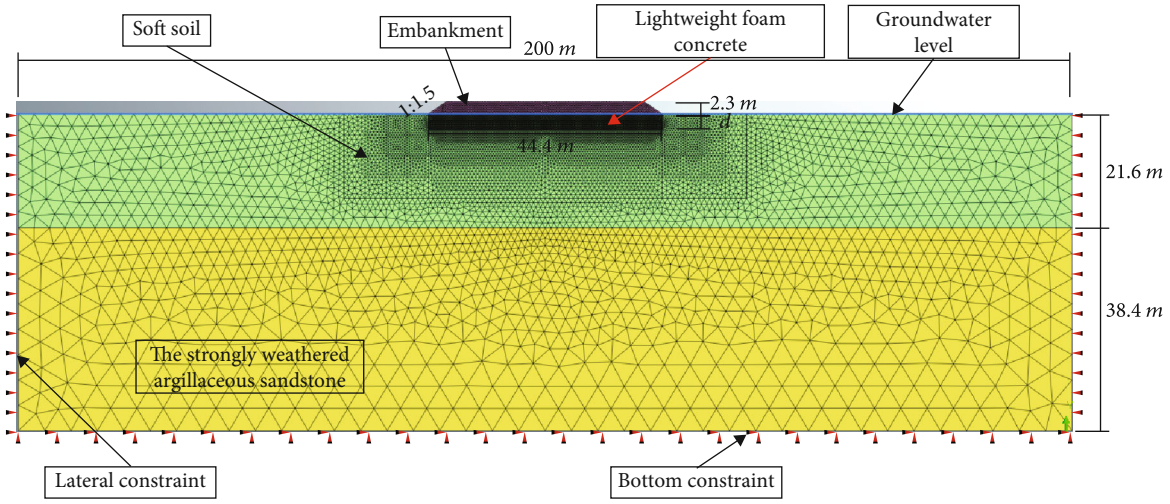

Figure 3: 2D finite element method model.

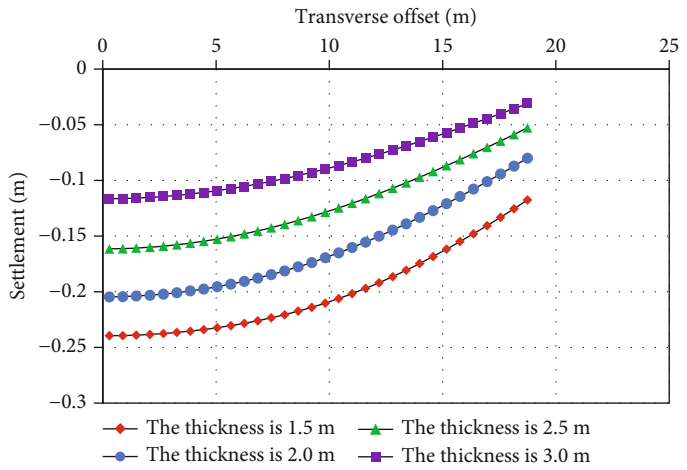

Figure 4: Settlement-transverse offset curves on the top of embankment with different thicknesses of replacement.

where **D** is the stress-strain relational matrix; $\mathbf{d}^e$ is the element node degree of freedom; and **N** is the shape function.

3.1.2. Seepage Analysis Theory. Unsteady-flow analysis was used in this study. The flow law used in MIDAS/GTS is Darcy's law, and the basic equation for flow is as follows [41]:

$$\frac{\partial}{\partial x}\left(k_x \frac{\partial H}{\partial x}\right) + \frac{\partial}{\partial y}\left(k_y \frac{\partial H}{\partial y}\right) + \frac{\partial}{\partial z}\left(k_z \frac{\partial H}{\partial z}\right) + Q = \frac{\partial \Theta}{\partial t}, \quad (4)$$

where H is the total head; k_x, k_y, and k_z are the permeability coefficient in the x-, y-, and z-directions, respectively; Q is the flow rate; Θ is the volumetric water content; and t is the time.

3.1.3. Mohr-Coulomb Strength Criterion. Mohr-Coulomb criterion is widely used, as the constitutive model can accurately reflect the characteristics of geotechnical materials. The equation of Mohr-Coulomb criterion is as follows [40]:

$$\frac{\sigma_1 - \sigma_3}{2 = -\sigma_1 + \sigma_3} \quad (5)$$
$$2 \sin \varphi + c \cos \varphi,$$

where σ_1 and σ_3 are the maximal and minimal principal stress, respectively; φ is the frictional angle; and c is the cohesion.

MIDAS/GTS assumes that the material satisfies the associative flow rule, and the yield criterion and plastic potential equations are as follows [44]:

$$\begin{cases} \frac{F(I_1, J_2, \theta_\sigma) = 1}{3} I_1 \sin \varphi + \sqrt{J_2}\left(\frac{\cos \theta_\sigma - 1}{\sqrt{3} \sin \theta_\sigma \sin \varphi}\right) - c \cos \varphi = 0, G(I_1, J_2, \theta_\sigma) = 1 \\ 3I_1 \sin \psi + \sqrt{J_2}\left(\frac{\cos \theta_\sigma - 1}{\sqrt{3} \sin \theta_\sigma \sin \psi}\right) - c \cos \psi = 0, \end{cases} \quad (6)$$

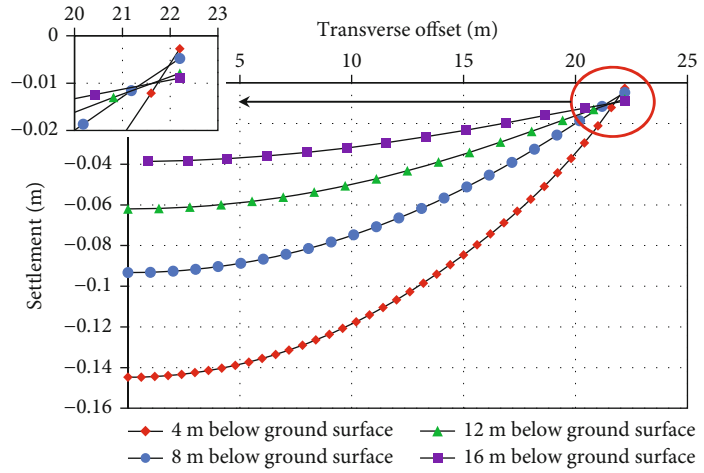

(a)

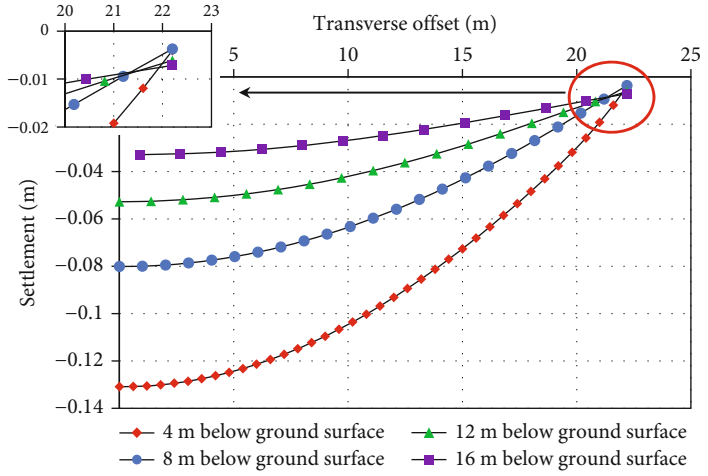

(b)

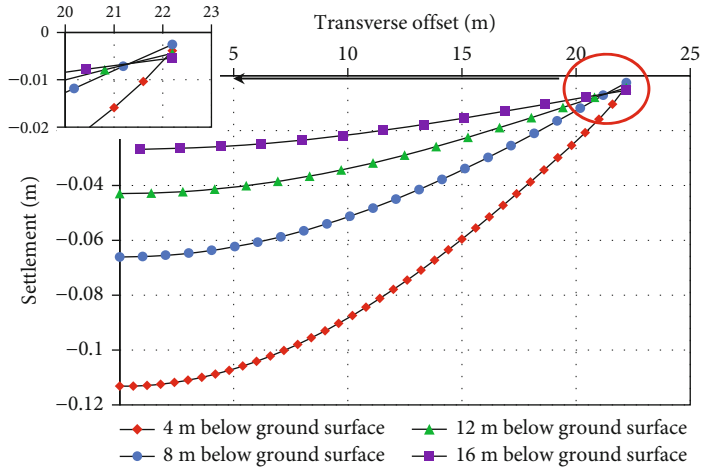

(c)

Figure 5: Continued.

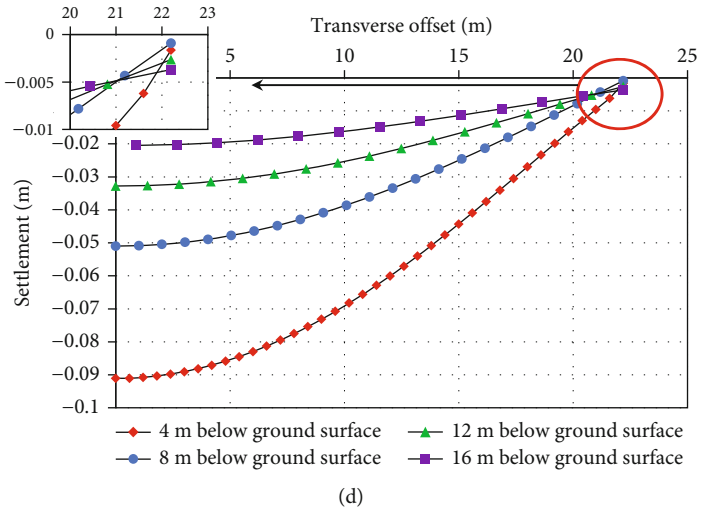

Figure 5: Settlement-transverse offset curve of different underground depths in the soft soil with the replacement thicknesses of (a) 1.5 m, (b) 2.0 m, (c) 2.5 m, and (d) 3.0 m.

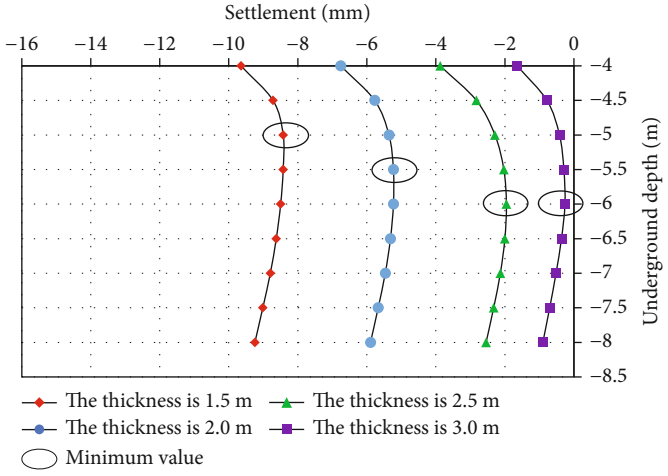

Figure 6: Settlements in the soft foundation of different underground depths under slope toe.

where I_1 is the first stress invariant; $J_2$is the second invariant of deviatoric stress; θ_σ is the Lode angle; and ψ is the dilatancy angle.

3.2. Models and Physical Parameters. Assuming that the transverse geology is invariant, the cross-sectional finite element model is established based on the geological interpretation of borehole 1 (Figure 3), with the width and height of 200 m and 60 m, respectively. The height and bottom width of the embankment are 2.3 m and 44.4 m, respectively. The thickness of the soft soil layer is 21.6 m, and the thicknesses of replacement are $d = 1.5, 2.0, 2.5, 3.0m$.

Element type: triangular plane strain element with six nodes

Initial conditions: in the present case, $\sigma_{zz} = \rho gz$ is the initial vertical stress in the z-direction; $\sigma_{xx} = \lambda_x \sigma_{zz}$ is the initial horizontal stresses in the x-direction. Moreover, the lateral total pressure coefficient is $\lambda_x = 1.0$

Boundary conditions: horizontal and vertical displacements are constrained at the bottom of the model, while horizontal displacements are constrained on both sides. A drainage boundary is set on the ground surface flush with the groundwater level. A total of 20 kPa traffic load is added on the top of the embankment uniformly after road completion.

Simulation steps include the geostress balance (steady-state analysis), construction of replacement and embankment, and 15-year opening to traffic.

The main parameters of materials are presented in Table 1. The parameters of soft soil and strongly weathered argillaceous sandstone are from the geological survey report, and the parameters of lightweight foam concrete and embankment are from the existing literature [9, 45–49].

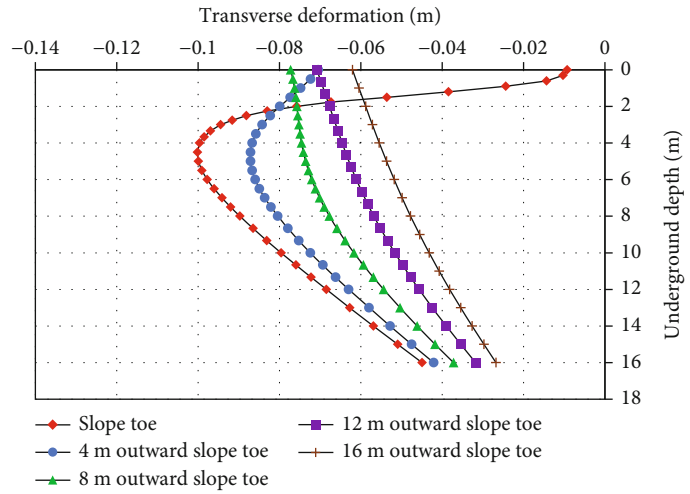

(a)

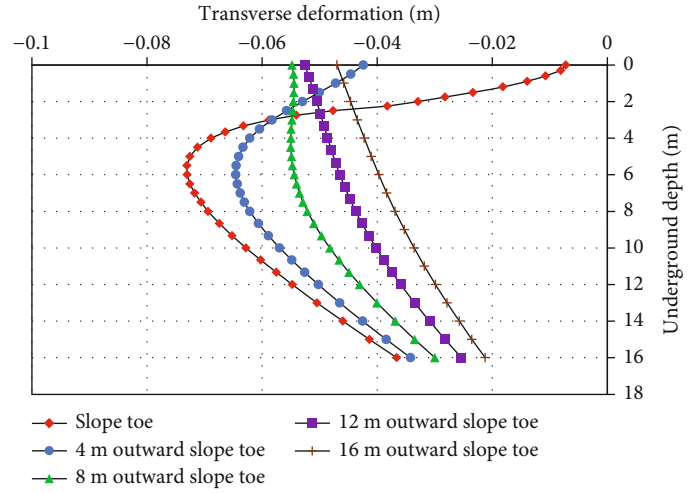

(b)

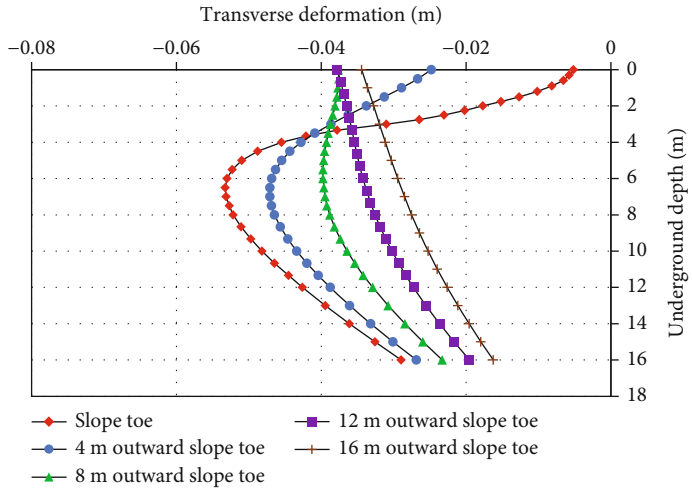

(c)

Figure 7: Continued.

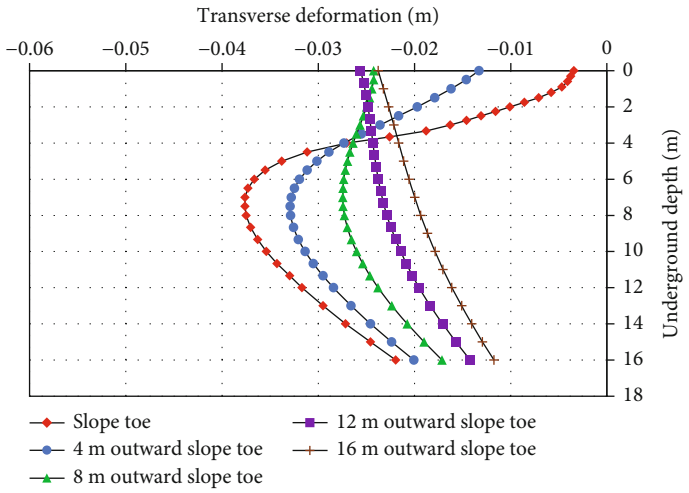

(d)

Figure 7: Transverse deformation-underground depth curves at different distances outside slope toe in soft soil with variable replacement thicknesses. (a) Replacement thickness = 1.5 m. (b) Replacement thickness = 2.0 m. (c) Replacement thickness = 2.5 m. (d) Replacement thickness = 3.0 m.

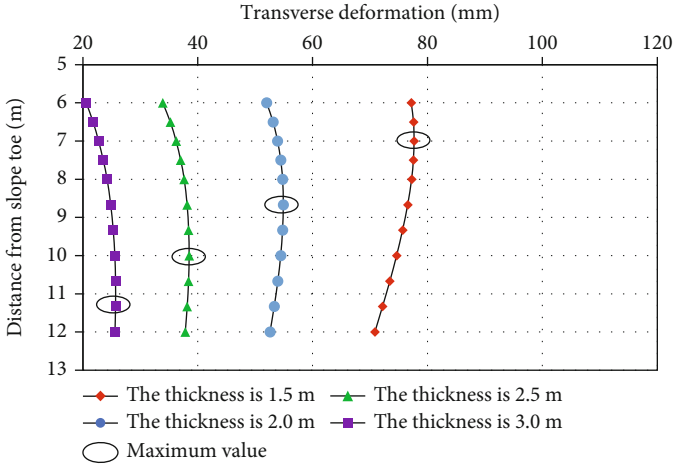

Figure 8: Transverse deformations at the ground surface with different distances from slope toe.

4. Result and Analysis

The simulation results of variables in this section are the final calculation results except for excess pore water pressure.

4.1. Deformation

4.1.1. Settlement. Figures 4 and 5 show the transverse settlement distribution on the embankment top and in the soft soil with different replacement thicknesses.

The following results are illustrated from Figure 4:

(1) The transverse settlement distribution of foundation and embankment presents an "arc" shape in cross-section, which is attributed to the closure effect [50] of replacement and flow deformation. Soft soil

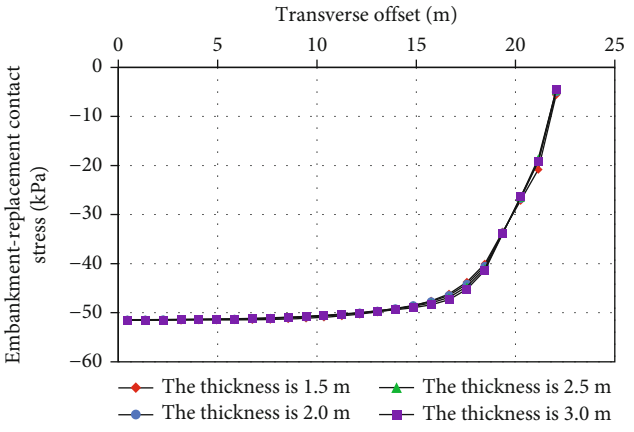

Figure 9: Transverse distribution of embankment-replacement contact stress with different thicknesses of replacement.

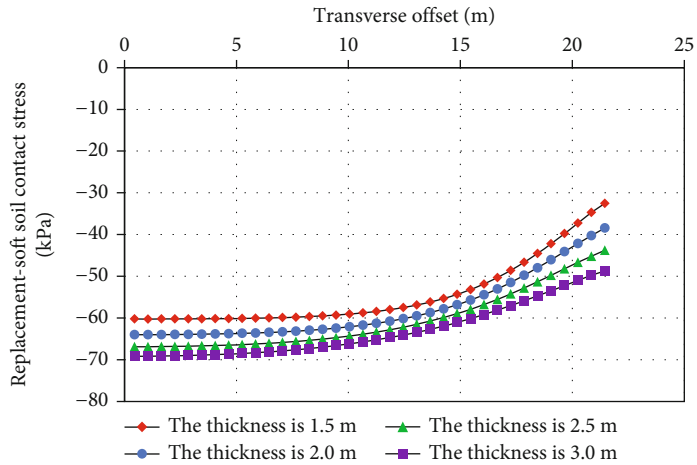

Figure 10: Transverse distribution of replacement-soft soil contact stress with different thicknesses of replacement.

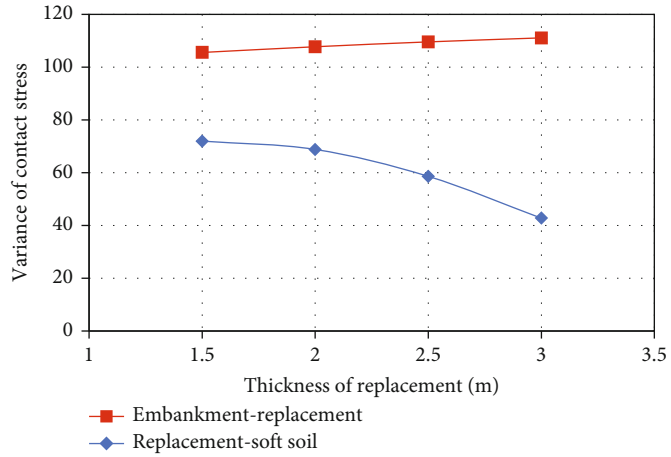

Figure 11: The variance of embankment-replacement and replacement-soft soil contact stresses with the increasing replacement thickness.

in the critical state will flow from the middle to both sides under the closure effect [50]

(2) The thicker the replacement, the smaller the settlement of embankment. When the thicknesses of replacement are 1.5, 2.0, 2.5, and 3.0 m, the maximum settlements on the top of the embankment are 23.95, 20.46, 16.20, and 11.64 cm, respectively. This is because the weight difference between soft soil and lightweight foam concrete is related to the replacement

The following result is illustrated from Figure 5:

(3) Generally, the settlement in the soft foundation under the embankment center decreases with the increasing underground depth, while that under slope toe performs differently (the results are extracted as shown in Figure 6)

It can be concluded from Figure 6 that an inflection point exists in the settlement-underground depth curve under the slope toe and gradually deepens with the increasing thickness of replacement. This is caused by the closure effect [50] of replacement and flow deformation of soft soil.

4.1.2. Transverse Deformation. Figure 7 shows the vertical distribution of transverse deformation in soft soil with different thicknesses of replacement.

The following results are illustrated from Figure 7:

(1) The transverse displacement in soft foundation decreases with the increasing thickness of replacement. When the thickness of replacement is 1.5, 2.0, 2.5, and 3.0 m, the maximum transverse displacement under slope toe is 10.02, 7.30, 5.32, and 3.76 cm, respectively. The same reason is depicted in Section 4.1.1 (2)

(2) The maximum transverse deformation moves downward as the thickness of the replacement increases. When the thicknesses are 1.5, 2.0, 2.5, and 3.0 m, the underground depths of the maximum transverse displacement under slope toe are 4.5, 5.5, 6.5, and 7.0 m, respectively. In addition, (3) the transverse

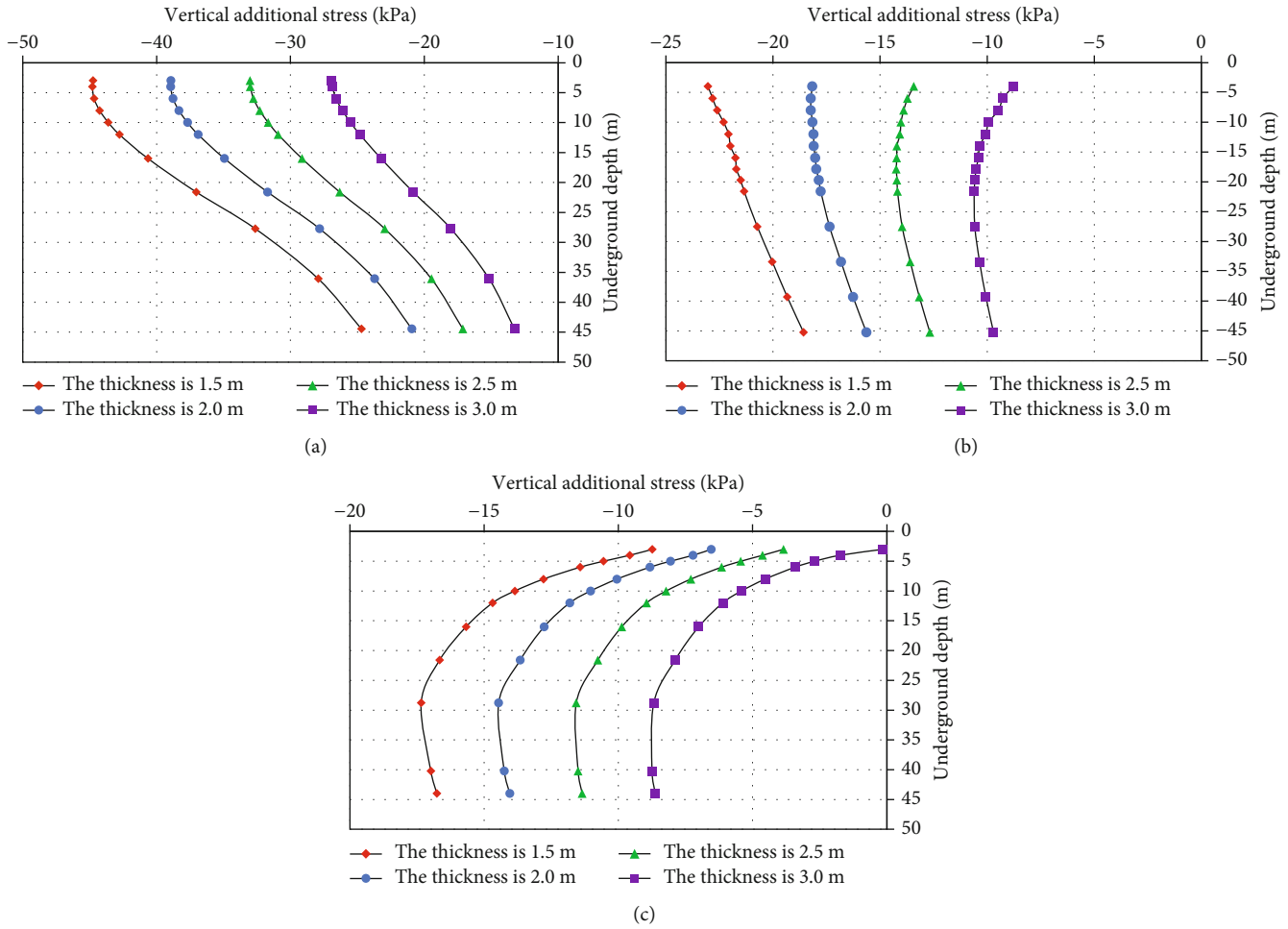

Figure 12: The vertical additional stress-underground depth curves with variable thickness of replacement under (a) embankment center, (b) embankment shoulder, and (c) slope toe.

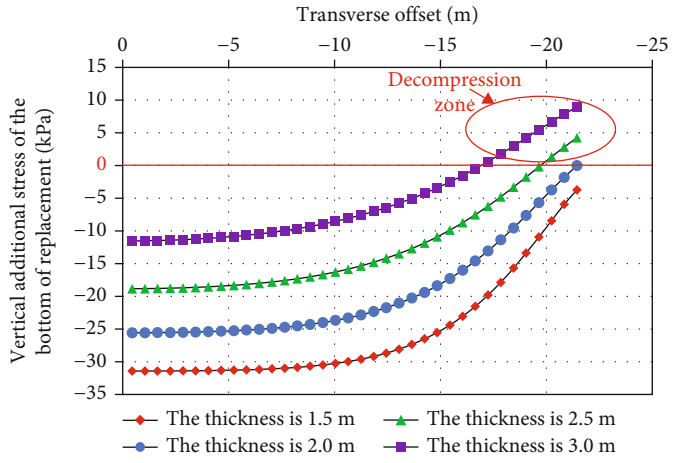

Figure 13: The transverse distribution of vertical additional stress on the bottom of replacement.

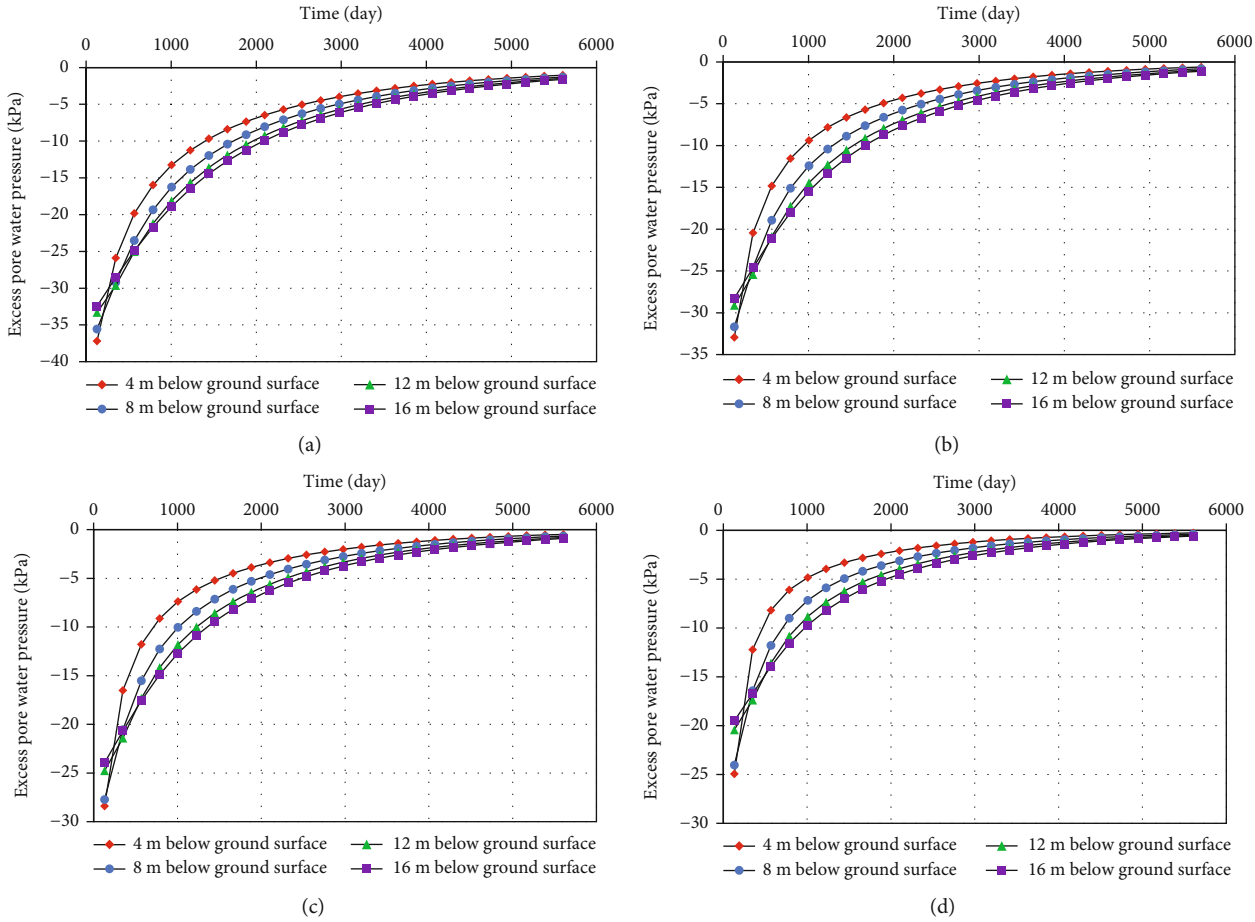

Figure 14: Excess pore water pressure-time curve in soft soil under embankment center with the replacement thicknesses of (a) 1.5 m, (b) 2.0 m, (c) 2.5 m, and (d) 3.0 m.

deformations at the ground surface outside slope toe are extracted, as shown in Figure 8

As shown in Figure 8, the maximum transverse displacement at the ground surface shifts outward with the increasing thickness of the replacement.

These phenomena (mentioned in viewpoints (2) and (3)) are relevant to the closure effect [50] of replacement and flow deformation.

4.2. Stress and Pressure

4.2.1. Contact Stress. Figures 9 and 10 show the transverse distributions of embankment-replacement and replacement-soft soil contact stress with different thicknesses of replacement, respectively.

The following results are illustrated from Figure 9:

(1) The transverse distribution of embankment-replacement contact stress presents a "trapezoid" shape, similar to the geometry of embankment. The centrifugal model test of Jiang et al. [51] verified this viewpoint. In addition, (2) the thickness of replacement is not the influencing factor of the embankment-replacement contact stress distribution.

The following results are illustrated from Figure 10:

(3) The distribution of replacement-soft soil contact stress gradually changes from the "trapezoid" to the "arc" shape with the increasing replacement thickness, implying the correlation between the spreading of the load and the thickness of replacement. The variance method is used to quantitatively analyze the influence of the replacement thickness on the stress diffusion. The variance of embankment-replacement and replacement-soft soil contact stresses are shown in Figure 11.

As shown in Figure 11, the uniformity of the distribution of replacement-soft soil contact stress increases with the rising thickness of replacement.

4.2.2. Vertical Additional Stress. Figure 12 shows the vertical distribution of vertical additional stress under embankment center, embankment shoulder, and slope toe with different thicknesses of replacement.

The following results are illustrated from Figure 12:

(1) The vertical additional stress in the soft soil decreases with the thickening replacement layer. For example, at 3 meters below the surface in Figure 12(a), when the thickness of replacement is 1.5, 2.0, 2.5, and 3.0 m, the vertical additional stress is 44.76, 38.94, 33.03, and

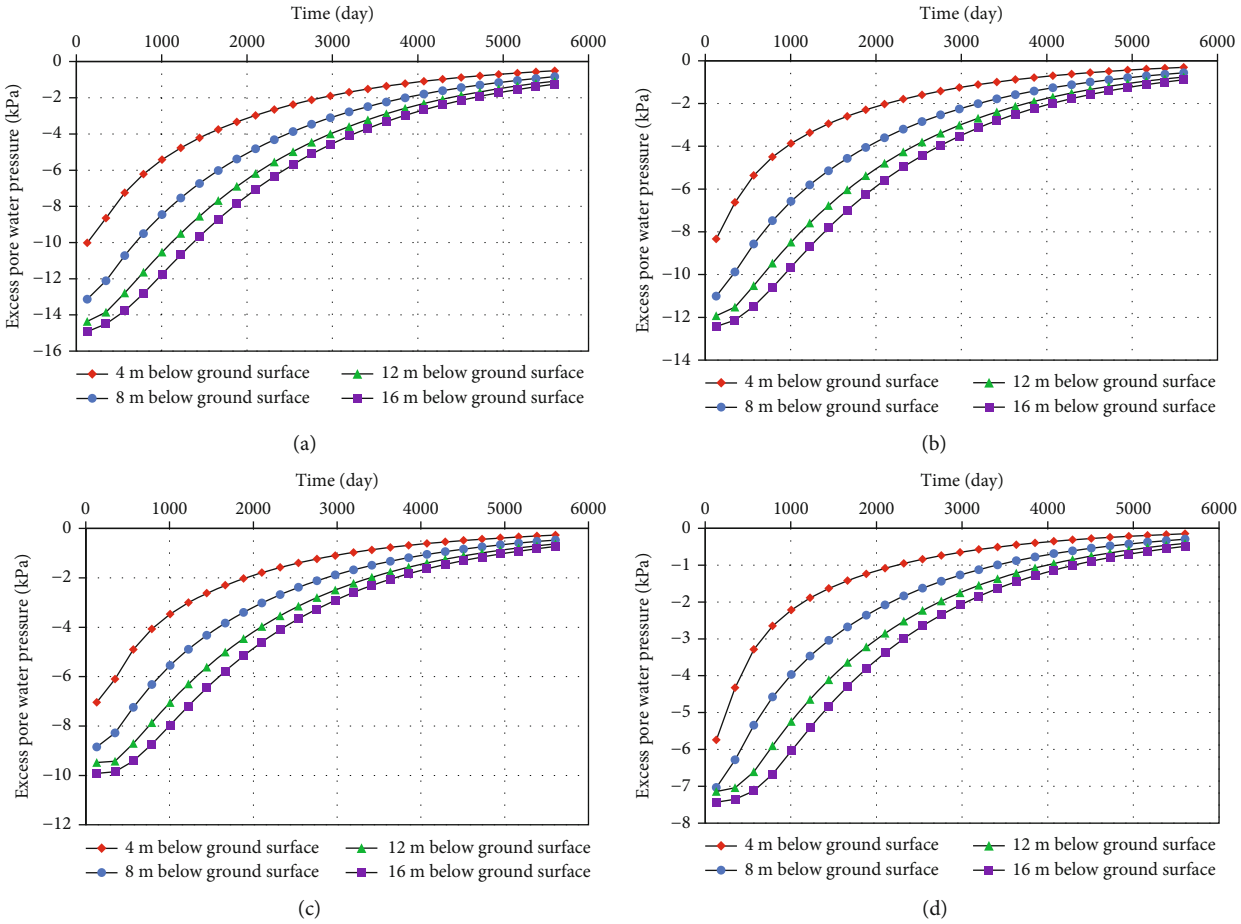

Figure 15: Excess pore water pressure-time curve in soft soil under slope toe with the replacement thicknesses of (a) 1.5 m, (b) 2.0 m, (c) 2.5 m, and (d) 3.0 m.

26.94 kPa, respectively. The reason is consistent with viewpoint (2) in Section 4.1.1

(2) The additional stress under the embankment center decreases with the deepened underground depth, and the gradient presents an increase firstly and then a decrease. The additional stress under the slope toe goes up and then down with the deepened underground depth. This is because the transverse shape of the additional stress contour is similar to a symmetrical "bubble" [52], and the axis of symmetry is at the embankment center

(3) When the replacement thickness is 1.5 and 2.0 m, the additional stress under the embankment shoulder decreases with the deepening of depth; when the thickness is 2.5 and 3.0 m, the additional stress under the embankment shoulder first increases and then decreases with the deepening of depth. This is because a decompression zone appears in the foundation (as shown in Figure 13, the new load on the bottom of replacement is less than the original load) when the replacement thickness is large, which results in the necking of the "bubble" around the bottom of replacement

4.2.3. Excess Pore Water Pressure. Figures 14 and 15 show the dissipation results of excess pore water pressure in soft soil under embankment center and slope toe, respectively, at the last calculation step.

The following results are illustrated from Figures 14 to 15:

(1) The greater the thickness of replacement, the lower the initial excess pore water pressure is. Taking the position 4 m below the surface in Figure 14 as an example: when the thicknesses of replacement are 1.5, 2.0, 2.5, and 3.0 m, the initial excess pore water pressures are 37.20, 32.94, 28.38, and 24.92 kPa, respectively. This is because the excess pore water pressure is caused by additional stress (the relationship between additional stress and thickness of replacement is depicted in viewpoint (1) of Section 4.2.2).

(2) The initial excess pore pressure under the embankment center gradually decreases with the deepening

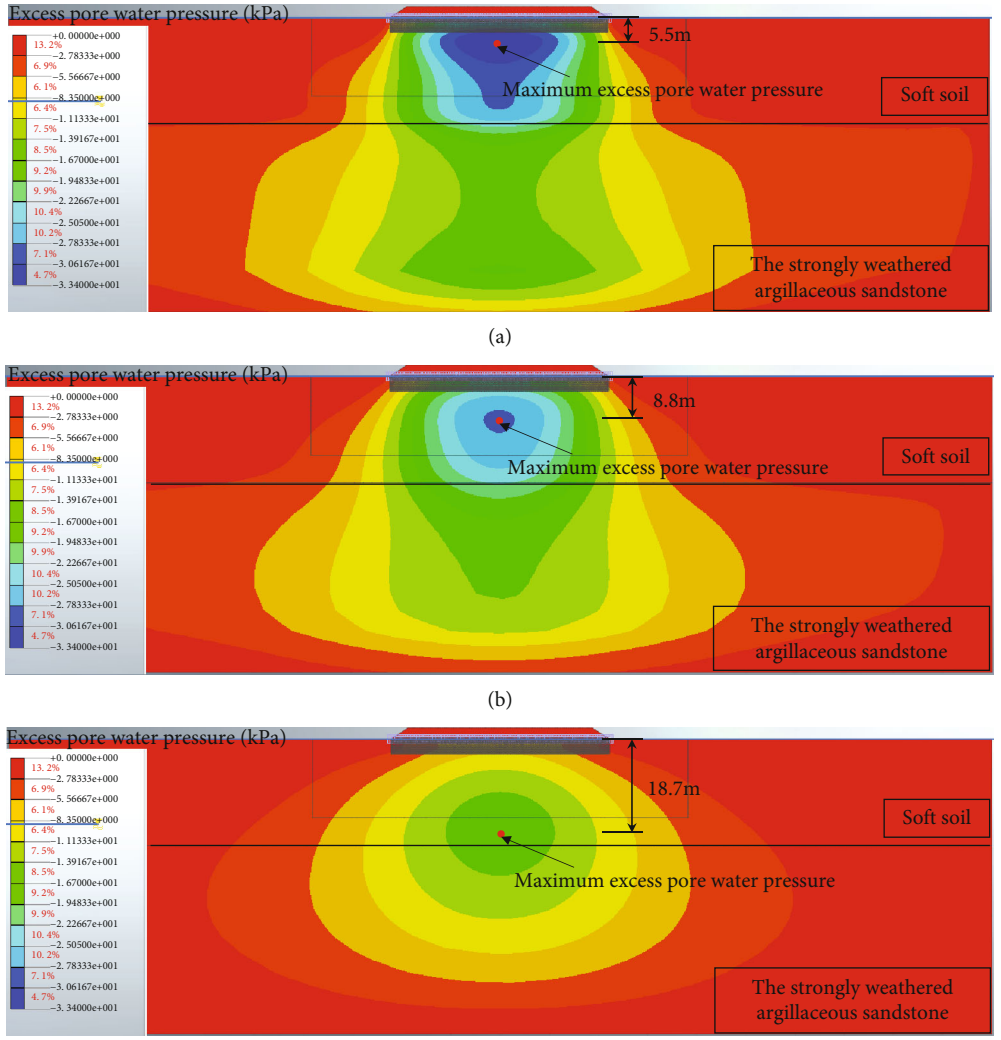

Figure 16: The colored nephogram of excess pore water pressure (a) four months, (b) seven months, and (c) twenty-nine months after road completion (the replacement thickness is 2 m).

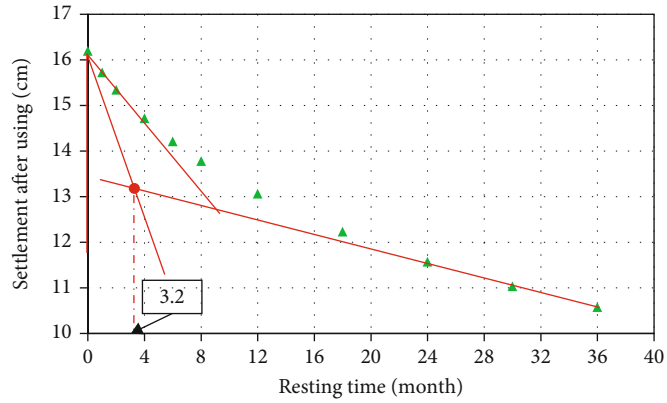

Figure 17: The relationship between settlement after 15 years of using and resting time.

of depth (4-16 m), while the initial excess pore pressure at the slope toe gradually increases with the deepening of depth (4-16 m). This phenomenon is related to the distribution of additional stress

(3) It can be concluded that the dissipation rate of excess pore water pressure is negatively correlated with underground depth by comparing the dissipation curves of excess pore water pressure of different underground depths. In addition, (4) the dissipation rate of excess pore water pressure under the embankment center is found greater than that under slope toe by comparing their dissipation curves. This may relate to dissipation path of excess pore water pressure

Figure 16 shows the colored nephogram of excess pore water pressure during the last calculation step (the replacement thickness is 2 m).

As shown in Figure 16, the position of the maximum excess pore water pressure gradually deepens with time. Considering the geometrically symmetric structure of the 2D model, the dissipation path of excess pore water pressure can be inferred to dissipate from the embankment center to both sides and downwards in the near field.

5. Preliminary Feasibility Analysis

The settlement, foundation bearing capacity, and stability of embankment slope are the main indicators for soft foundation reinforcement design in road engineering [9]. This paper focuses on the low-filled embankment, and thus, the instability of the embankment slope is unimportant. Furthermore, given that the volume weight of lightweight foam concrete is less than that of water, the antifloating stability is given additional consideration [37].

In this section, the calculation results of settlement, foundation bearing capacity, and antifloating stability are obtained for the final replacement thickness of this project (2.5 m, considering safety and construction factors), and the optimal resting time is suggested.

5.1. Settlement. The maximum settlement on the top of the embankment with different thicknesses of replacement is listed in Figure 4. When the replacement thickness is 2.5 m, the settlement meets the requirements of general highway sections in the existing technical specification (16.20 cm<30 cm) [9]. Therefore, the settlement of soft foundation handled by LFCRM accords with the existing technical specification.

5.2. Foundation Bearing Capacity. The maximum replacement-soft soil contact stress with a thickness of 2.5 m can be obtained from Figure 10, which is 66.90 kPa. The foundation bearing capacity is calculated according to Terzaghi's equation [53] (Equation (7)), and the result show the reasonability of the bearing capacity.

$$p_u = 1/2\gamma b N_\gamma + cN_c + qN_q, \tag{7}$$

where γ is soft soil weight; b is footing width; N_γ, N_c, and N_q are dimensionless coefficients; c is the cohesion of soft soil; and q is specific soil pressure above footing bottom. The footing width item in Equation (7) is not considered in this paper.

5.3. Antifloating Stability. Only the permanent load is considered in calculating antifloating stability (as shown in Equation (8)), and the safety factor is no less than 1.2 [37]. Taking an example for calculation (the thickness of replacement is 2.5 m and the groundwater level is flush with the top of the embankment), the calculation result meets the requirements [37].

$$\frac{F_s = 0.95\sum_{i=1}^{n}\gamma_i V_i}{\rho_w g V_w \geq 1.2,} \tag{8}$$

where γ_i is the volume weight of filling materials; V_i is the volume of filling materials; $\rho_w g$ is the volume weight of groundwater; and V_w is the volume of filling under the groundwater level.

According to above preliminary analysis, it is feasible to treat the deep soft foundation with the low-filled embankment by LFCRM.

5.4. Resting Time after Road Completion. Figure 17 shows the relationship between resting time (the time between completion and using of road) and the total settlement after 15 years of using. It can be seen from the figure that with the increase of resting time, the total settlement after using gradually decreases, and the rate of decrease is also slowing down. The abrupt change point of the curve, 3.2 months (about 96 days), is calculated by the Casagrande method [54] as the optimal resting time.

It should be pointed out that LFCRM is not suitable for all conditions. According to the existing research results, this paper believes that the following conditions may not be suitable: (1) high-filled embankment sections, (2) areas with obvious alternate cooling and heating (around 0 degrees Celsius) [55], and (3) saline land [56].

6. Conclusions

The result of deep soft foundation with low-filled embankment improved by LFCRM with different thicknesses of replacement is obtained using the finite element method, and the deformation and stress of the numerical results are analyzed in detail. Finally, the preliminary feasibility of LFCRM is demonstrated by combining the numerical results and the Chinese technical specification [9, 37]. The detailed conclusions are as follows:

(i) Replacing soft soil with lightweight foam concrete can offset part of dead load due to the weight difference between the two materials, reducing the deformation, additional stress, and initial excess pore water pressure accordingly. This feature will be enhanced by the increasing thickness of replacement

(ii) The transverse distribution of settlement of embankment and foundation presents an "arc" shape under the combined action of flow of soft soil and the closure effect of replacement

(iii) The uniformity of the replacement-soft soil contact stress is significantly better than that of the embankment-replacement contact stress due to the stress spreading

(iv) A decompression zone appears in the foundation with the replacement thickness increases and results in the necking of the "bubble" around the bottom of replacement

(v) The distribution of initial excess pore water pressure is relevant to additional stress, and excess pore water pressure will dissipate from the center to both sides of embarkment and downwards in the near field

(vi) LFCRM is preliminarily considered feasible by analyzing settlement, foundation bearing capacity, and antifloating stability based on numerical results and Chinese technical specification, and the optimal resting time is suggested

In the next step in the future, the feasibility of LFCRM will be further studied by field test.

Data Availability

The data used to support the findings of this study are available from the corresponding author upon request.

Additional Points

Featured Application. New method for treating deep soft foundation treatment with low-filled embankment. *Highlight*. (i) A new method, lightweight foam concrete replacement method (LFCRM), is carried out to treat deep soft foundations under the low-filled embankment; (ii) LFCRM can offset and spread the upper load effectively which is related to replacement thickness; (iii) the deformation of treated foundation is affected by flow of soft soil and closure effect of replacement; (iv) the excess pore water pressure will dissipate from the center to both sides of embarkment and downwards in the near field; (v) the potential feasibility of LFCRM is demonstrated by preliminary analysis.

Conflicts of Interest

The authors declare that they have no known competing financial interests or personal relationships that could have appeared to influence the work reported in this paper.

Authors' Contributions

Conceptualization was performed by Fanfan Li and Zecheng Chi; formal analysis was performed by Fanfan Li and Xing Chen; investigation was performed by Fanfan Li and Zhifeng Zhang; resources were contributed by Zhifeng Zhang; supervision was contributed by Zecheng Chi; visualization was performed by Fanfan Li; writing–original draft was contributed by Fanfan Li; writing–review and editing was contributed by Fanfan Li, Zhifeng Zhang, Xing Chen, Zecheng Chi, Jianbin Li, and Wei Wang.

Acknowledgments

This research is funded by the National Natural Science Foundation of China, grant numbers 52008122 and 52108366; the China Postdoctoral Science Foundation, grant number 51479190; and the Science and Technology Project of Housing Urban and Rural Construction in Anhui Province, grant number 2020-YF19;

References

[1] M. Zhou, F. Dang, Y. Li, J. Ding, J. Gao, and C. Wu, "Study on critical hydraulic gradient theory of flow soil failure in cohesive soil foundation," *Geofluids*, vol. 2021, Article ID 5599977, 13 pages, 2021.

[2] X. Fu, Q. Sheng, G. Li, Z. Zhang, Y. Zhou, and Y. Du, "Analysis of landslide stability under seismic action and subsequent rainfall: a case study on the Ganjiazhai giant landslide along the Zhaotong-Qiaojia road during the 2014 Ludian earthquake, Yunnan, China," *Bulletin of Engineering Geology and the Environment*, vol. 79, no. 10, pp. 5229–5248, 2020.

[3] Y. Zhou, Q. Sheng, N. Li, and X. Fu, "The dynamic mechanical properties of a hard rock under true triaxial damage-controlled dynamic cyclic loading with different loading rates: a case study," *Rock Mechanics and Rock Engineering*, vol. 55, no. 4, pp. 2471–2492, 2022.

[4] Y. Mei, D. Zhou, X. Wang et al., "Deformation law of the diaphragm wall during deep foundation pit construction on Lake and sea soft soil in the Yangtze River Delta," *Advances in Civil Engineering*, vol. 2021, 11 pages, 2021.

[5] L. Lou, *Study on Key Technologies of Deep Soft Soil Foundation Treatment and Low Embankment Design of Highway (in Chinese),. Master*, Southwest Jiaotong University, 2016.

[6] C. Lee, C. Lau, C. Ng et al., *Soft Soil Engineering. 1st Editon Ed*, Routledge, London, Greater London, United Kingdom, 2001.

[7] L. Miao, F. Wang, and W. Lv, "A simplified calculation method for stress concentration ratio of composite foundation with rigid piles," *KSCE Journal of Civil Engineering*, vol. 22, no. 9, pp. 3263–3270, 2018.

[8] Y. Wang, X. Zou, and J. Hu, "Bearing capacity of single pile-friction wheel composite foundation on sand-over-clay deposit under V-H-M combined loadings," *Applied Sciences*, vol. 11, no. 20, p. 9446, 2021.

[9] MOT, *Technical Guidelines for Design and Construction of Highway Embankment on Soft Ground (in Chinese) JTG/T D31-02-2013 General Office of Ministry of Transport*, Ministry of Transport of the People's Republic of China (MOT), Beijing, China, 2013.

[10] T. Yang, J. Z. Yang, and J. Ni, "Analytical solution for the consolidation of a composite ground reinforced by partially penetrated impervious columns," *Computers and Geotechnics*, vol. 57, pp. 30–36, 2014.

[11] Y. G. Zhang, M. Sun, and K. H. Xie, "Study of simplifying solution to consolidation of composite ground with partially penetrated granular columns (in Chinese)," *Rock and Soil Mechanics*, vol. 35, no. 5, 2014.

[12] S. Rajesh, "Time-dependent behaviour of fully and partially penetrated geosynthetic encased stone columns," *Geosynthetics International*, vol. 24, no. 1, pp. 60–71, 2017.

[13] S. Yan, J. Chen, L. Sun, H. Chen, and S. Lin, "Calculation method and model test on penetration depth of squeezing soft

clay (with stone) method (in Chinese)," *Rock and Soil Mechanics*, vol. 36, pp. 43–48, 2015.

[14] J. C. Chai, J. P. Carter, and S. Hayashi, "Vacuum consolidation and its combination with embankment loading," *Canadian Geotechnical Journal*, vol. 43, no. 10, pp. 985–996, 2006.

[15] J. Hu, X. Li, D. Zhang, J. Wang, X. Hu, and Y. Cai, "Experimental study on the effect of additives on drainage consolidation in vacuum preloading combined with electroosmosis," *KSCE Journal of Civil Engineering*, vol. 24, no. 9, pp. 2599–2609, 2020.

[16] Y. Huang, T. Li, and X. Fu, "Consolidation of unsaturated drainage well foundation with smear effect under time-dependent loading," *KSCE Journal of Civil Engineering*, vol. 25, no. 3, pp. 768–781, 2021.

[17] TRB, *Treatment of Soft Foundations for Highway Embankments*, Transportation Research Board (TRB), 1975, http://trb.org/Onlinepubs/nchrp/nchrp_syn_29.pdf.

[18] H. Y. Fang, *Foundation Engineering Handbook. 2nd Edition Ed*, Springer US, New York, NY, USA, 1991.

[19] Y. Wang, Y. Chen, W. Qiao, D. Zuo, Z. Hu, and Q. Feng, "Road engineering field tests on an artificial crust layer combined with pre-stressed pipe piles over soft ground," *Soil Mechanics and Foundation Engineering*, vol. 54, no. 6, pp. 402–408, 2018.

[20] M. B. Burbank, T. J. Weaver, T. L. Green, B. C. Williams, and R. L. Crawford, "Precipitation of calcite by indigenous microorganisms to strengthen liquefiable soils," *Geomicrobiology Journal*, vol. 28, no. 4, pp. 301–312, 2011.

[21] S. L. Zhan, S. S. Gao, and J. Y. Lai, "Research about the effect of polypropylene fiber on mechanical properties of curing sludge," *Advanced Materials Research*, vol. 250-253, pp. 788–794, 2011.

[22] D. M. Burmister, "The general theory of stresses and displacements in layered systems. I," *Journal of Applied Physics*, vol. 16, no. 2, pp. 89–94, 1945.

[23] C. T. Tam, T. Y. Lim, R. S. Ravindrarajah, and S. L. Lee, "Relationship between strength and volumetric composition of moist-cured cellular concrete," *Magazine of Concrete Research*, vol. 39, no. 139, pp. 115–115, 1987.

[24] E. K. K. Nambiar and K. Ramamurthy, "Sorption characteristics of foam concrete," *Cement and Concrete Research*, vol. 37, no. 9, pp. 1341–1347, 2007.

[25] C. Bing, W. Zhen, and L. Ning, "Experimental research on properties of high-strength foamed concrete," *Journal of Materials in Civil Engineering*, vol. 24, no. 1, pp. 113–118, 2012.

[26] G. I. S. Ranjani and K. Ramamurthy, "Behaviour of foam concrete under sulphate environments," *Cement and Concrete Composites*, vol. 34, no. 7, pp. 825–834, 2012.

[27] K. Wan, G. Li, S. Wang, and C. Pang, "3D full field study of drying shrinkage of foam concrete," *Cement and Concrete Composites*, vol. 82, pp. 217–226, 2017.

[28] Z. Q. Zhang and J. L. Yang, "Improving safety of runway overrun through foamed concrete aircraft arresting system: an experimental study," *International Journal of Crashworthiness*, vol. 20, no. 5, pp. 448–463, 2015.

[29] X. Tan, W. Chen, H. Liu et al., "A combined supporting system based on foamed concrete and U-shaped steel for underground coal mine roadways undergoing large deformations," *Tunnelling and Underground Space Technology*, vol. 68, pp. 196–210, 2017.

[30] W. She, Y. Du, G. Zhao, P. Feng, Y. Zhang, and X. Cao, "Influence of coarse fly ash on the performance of foam concrete and its application in high-speed railway roadbeds," *Construction and Building Materials*, vol. 170, pp. 153–166, 2018.

[31] D. G. Cai, S. W. Wei, Y. S. Ye, Q. L. Zhang, Z. G. Li, and S. Li, "Mechanical properties of lightweight foam concrete filler for roadbed of high-speed railway," *Arabian Journal of Geosciences*, vol. 14, no. 10, 2021.

[32] J. Huang, Q. Su, W. Zhao, T. Li, and X. Zhang, "Experimental study on use of lightweight foam concrete as subgrade bed filler of ballastless track," *Construction and Building Materials*, vol. 149, pp. 911–920, 2017.

[33] T. Klomranok and Q. Su, "Assessment of the use of polypropylene fiber reinforced foam concrete as a subgrade material for the China Railway Track System (CRTS) III slab ballastless tracks," *Transportation Research Record: Journal of the Transportation Research Board*, vol. 2675, no. 11, pp. 641–654, 2021.

[34] A. Hajimohammadi, T. Ngo, and P. Mendis, "Enhancing the strength of pre-made foams for foam concrete applications," *Cement and Concrete Composites*, vol. 87, pp. 164–171, 2018.

[35] A. Raj, D. Sathyan, and K. M. Mini, "Physical and functional characteristics of foam concrete: a review," *Construction and Building Materials*, vol. 221, pp. 787–799, 2019.

[36] E. Eltayeb, X. Ma, Y. Zhuge, O. Youssf, and J. E. Mills, "Influence of rubber particles on the properties of foam concrete," *Journal of Building Engineering*, vol. 30, p. 101217, 2020.

[37] MOHURD, "Technical Specification for Foamed Mixture Lightweight Soil Filling Engineering (in Chinese) CJJ/T 177-2012 Ministry of Housing and Urban Rural Development of the People's Republic of China (MOHURD) Beijing, China," in *China Architecture and Building Press*, 2012.

[38] J. H. Hu, T. Lei, K. P. Zhou, X. W. Luo, and N. G. Yang, "Mechanical response of roof rock mass unloading during continuous mining process in underground mine," *Transactions of Nonferrous Metals Society of China*, vol. 21, no. 12, pp. 2727–2733, 2011.

[39] L. Duris and E. Hrubesova, "Numerical simulation of the interaction between fibre concrete slab and subsoil—the impact of selected determining factors," *Sustainability*, vol. 12, no. 23, 2020.

[40] X. Gao, W. Tian, and Z. Zhang, "Analysis of deformation characteristics of foundation-pit excavation and circular wall," *Sustainability*, vol. 12, no. 8, 2020.

[41] C. Yuan, Z. Hu, Z. Zhu et al., "Numerical simulation of seepage and deformation in excavation of a deep foundation pit under water-rich fractured intrusive rock," *Geofluids*, vol. 2021, Article ID 6628882, 10 pages, 2021.

[42] J. Xue, J. Lin, B. Briseghella, H. Tabatabai, and B. Chen, "Solar radiation parameters for assessing temperature distributions on bridge cross-sections," *Applied Sciences*, vol. 8, no. 4, 2018.

[43] H. Stolarski and T. Belytschko, "On the equivalence of mode decomposition and mixed finite elements based on the hellinger-reissner principle. Part I: theory," *Computer Methods in Applied Mechanics and Engineering*, vol. 58, no. 3, pp. 249–263, 1986.

[44] H. S. Yu, *Plasticity and Geotechnics*, Springer US, New York, NY, USA, 2006.

[45] R. W. Crossley and G. H. Beckwith, *Subgrade Elastic Modulus for Arizona Pavements*, 1978.

[46] W. Wei, W. Qin, and X. Fan, "Testing method of elastic modulus of foamed concrete (in Chinese)," *Concrete*, vol. 9, pp. 4–

6, 2008, http://www.cnki.com.cn/Article/CJFDTotal-HLTF200809002.htm.

[47] S. Meena, L. Choudhary, and A. Dey, "Quasi-static analysis of geotextile reinforced unpaved road resting on _c-φ_ subgrade," *Procedia-Social and Behavioral Sciences*, vol. 104, pp. 235–244, 2013.

[48] N. Sutmoller, M. Gomez, and J. Kevern, "Soft soil remediation with permeable low-density cellular concrete (PLDCC)," *MATEC Web of Conferences*, vol. 271, p. 02002, 2019.

[49] MOT, *Specifications for Design of Highway Subgrades (in Chinese) JTG D30-2015 General Office of Ministry of Transport*, Ministry of Transport of the People's Republic of China (MOT), Beijing, China, 2015.

[50] Y. X. Wen and J. Zhou, "Critical edge pressure analysis of two-layered ground considering closure effect (in Chinese)," *Chinese Journal of Geotechnical Engineering*, vol. 30, pp. 685–689, 2008.

[51] L. Jiang, H. Wang, A. Li, and C. Zhang, "Experimental study on ground reaction under loading of soil subgrade (in Chinese)," *Journal of the China Railway Society*, vol. 34, pp. 69–74, 2012.

[52] G. L. Wang, S. Y. Qu, X. M. Hou, F. F. Zhu, and J. Zhang, "Preliminary study on vertical subsoil participating mass," *Advanced Materials Research*, vol. 199-200, pp. 1429–1434, 2011.

[53] V. G. Fedorovskii, "A correction term in the Terzaghi equation for subsoil bearing capacity analysis," *Soil Mechanics and Foundation Engineering*, vol. 53, no. 6, pp. 365–369, 2017.

[54] A. O. Eberemu, "Consolidation properties of compacted lateritic soil treated with rice husk ash," *Geomaterials*, vol. 1, no. 3, pp. 70–78, 2011.

[55] X. Tan, W. Chen, H. Tian, and J. Yuan, "Degradation characteristics of foamed concrete with lightweight aggregate and polypropylene fibre under freeze–thaw cycles," *Magazine of Concrete Research*, vol. 65, no. 12, pp. 720–730, 2013.

[56] Y. Lei, *Experimental Study on Salt Corrosion Resistance of Lightweight Cement Fly Ash Subgrade Filler (in Chinese)*, Taiyuan University of Technology, 2020.